View metadata, citation and similar papers at core.ac.uk
brought to you by CORE
provided by Elsevier - Publisher Connector

Cell

Peptidoglycan Crosslinking Relaxation Promotes *Helicobacter pylori*'s Helical Shape and Stomach Colonization

Laura K. Sycuro,[1,3] Zachary Pincus,[4] Kimberley D. Gutierrez,[2] Jacob Biboy,[5] Chelsea A. Stern,[2,3] Waldemar Vollmer,[5] and Nina R. Salama[2,3,*]
[1]Molecular and Cellular Biology Graduate Program
[2]Department of Microbiology
University of Washington, Seattle, WA 98195, USA
[3]Division of Human Biology, Fred Hutchinson Cancer Research Center, Seattle, WA 98109, USA
[4]Department of Molecular, Cellular, and Developmental Biology, Yale University, New Haven, CT 06520, USA
[5]Centre for Bacterial Cell Biology, Institute for Cell and Molecular Biosciences, Newcastle University, Newcastle upon Tyne NE2 4HH, UK
*Correspondence: nsalama@fhcrc.org
DOI 10.1016/j.cell.2010.03.046

SUMMARY

The mechanisms by which bacterial cells generate helical cell shape and its functional role are poorly understood. Helical shape of the human pathogen *Helicobacter pylori* may facilitate penetration of the thick gastric mucus where it replicates. We identified four genes required for helical shape: three LytM peptidoglycan endopeptidase homologs (*csd1–3*) and a *ccmA* homolog. Surrounding the cytoplasmic membrane of most bacteria, the peptidoglycan (murein) sacculus is a meshwork of glycan strands joined by peptide crosslinks. Intact cells and isolated sacculi from mutants lacking any single *csd* gene or *ccmA* formed curved rods and showed increased peptidoglycan crosslinking. Quantitative morphological analyses of multiple-gene deletion mutants revealed each protein uniquely contributes to a shape-generating pathway. This pathway is required for robust colonization of the stomach in spite of normal directional motility. Our findings suggest that the coordinated action of multiple proteins relaxes peptidoglycan crosslinking, enabling helical cell curvature and twist.

INTRODUCTION

The abundant morphological diversity present among bacteria has long been appreciated by microbiologists. Yet only recently has much progress been made toward understanding the mechanisms responsible for generating distinctive cell shapes (Young, 2006; Cabeen and Jacobs-Wagner, 2007). To date, most studies have focused on a select group of model organisms representing the most common shapes: rod (*Escherichia coli* and *Bacillus subtilis*), coccoid (*Staphylococcus aureus* and *Streptococcus* species), and vibrioid (or curved rod; *Caulobacter crescentus*). The machinery giving rise to cell shape in helical bacteria remains largely unknown. An exception is the *Spiroplasma* cytoskeletal apparatus, composed predominantly of Fib, a protein found in only a few prokaryotic species (Williamson et al., 1991), and MreB, a common prokaryotic cytoskeletal protein homologous to eukaryotic actin (Jones et al., 2001; Bove et al., 2003; Daniel and Errington, 2003). Fib, possibly in conjunction with MreB, forms bundles of filaments in a ribbon-like helix, which attaches to the inner surface of the membrane along the shortest (inner) helical line and twists the cell into a helix (Trachtenberg, 2004; Trachtenberg et al., 2008).

Spiroplasma, however, belong to an unusual class of bacteria, the Mollicutes, which lack the rigid cell wall known as the peptidoglycan (PG, or murein) sacculus. The exocellular sacculus surrounds the cytoplasmic membrane of most bacteria and is composed of stiff glycan strands crosslinked by flexible peptide bridges to form a mesh structure (Vollmer and Bertsche, 2008). PG prevents cell lysis due to turgor pressure and is required to maintain bacterial cell shape. Isolated PG sacculi also retain the morphology of the intact cell (Vollmer and Bertsche, 2008). A group of walled bacteria in which some progress has been made toward understanding helical shape determination is *Spirochetes*. These bacteria house flagella in the periplasmic space between the inner and outer membranes that are sometimes required for helical cell shape (Goldstein et al., 1994). Periplasmic flagella presumably act as force-generating cytoskeletal elements that bend the cell into a helix (Wolgemuth et al., 2006). However, some *Spirochete* species retain helical morphology in the absence of periplasmic flagella and the cellular machinery involved in generating their helicity has yet to be identified (Bromley and Charon, 1979; Ruby et al., 1997).

Here we investigate the helical shape of *Helicobacter pylori*. *H. pylori* is a member of the Epsilonproteobacteria, a class of bacteria composed almost exclusively of helical and curved organisms. *H. pylori*'s habitat is the human stomach, which it colonizes in approximately 50% of the world population. *H. pylori* infection is associated with the development of chronic gastric inflammation that can lead to ulcers and gastric cancer in

a subset of those infected (Kusters et al., 2006). *H. pylori*'s helical cell shape is conserved in human isolates (Goodwin et al., 1985), although the pitch of the helix varies among laboratory strains (L.K.S., unpublished data). This has given rise to the hypothesis that *H. pylori*'s helical shape serves an important function in pathogenesis (Montecucco and Rappuoli, 2001; Cover and Blaser, 2009). The prevailing theory is that helical shape enhances *H. pylori*'s flagellar motility through the viscous epithelial mucus layer in which it resides by a corkscrew mechanism (Hazell et al., 1986).

Helical cell shape can be thought of as the sum of three morphogenic components: cell elongation, curvature, and twist. Recent studies of the Gram-negative model organisms *E. coli* and *C. crescentus* have provided significant insight into the genes and mechanisms these species use to elongate the cell body and generate curvature. Although *H. pylori* encodes some of these genes, others appear to be absent or too highly divergent for sequence-based identification. Specifically, *H. pylori* encodes all three of the high-molecular-weight penicillin-binding proteins (PBPs) required for PG glycan synthesis (transglycosylation via PBP1) and peptide crosslinking (transpeptidation via PBP1, PBP2, and PBP3) (Tomb et al., 1997; DeLoney and Schiller, 1999). However, low-molecular-weight PBPs with endopeptidase and/or carboxypeptidase activities that contribute to PG hydrolysis and postsynthetic modification of crosslinked and uncrosslinked peptide chains have not been identified in *H. pylori*. In *E. coli* and *C. crescentus*, cell body elongation requires the actin homolog MreB, which, in conjunction with other cytoskeletal filaments and scaffolding proteins (i.e., FtsZ, MreC, MreD, RodA, and RodZ), appears to spatially position PG synthesis in roughly helical bands or patches along the cell body, resulting in rod elongation (Cabeen and Jacobs-Wagner, 2007; Alyahya et al., 2009; Bendezu et al., 2009). Although *H. pylori* encodes all of these proteins, their role in elongating the *H. pylori* cell body has not been confirmed. CreS, an intermediate filament homolog in *C. crescentus*, is required for that organism's cell curvature (Ausmees et al., 2003). Through interactions with MreB, the CreS filament is tethered longitudinally along the inner membrane, creating a growth differential that limits PG synthesis rates along the CreS-lined sidewall and enables faster rates along the opposite sidewall, thus forming a curved cell body (Cabeen et al., 2009). Intermediate filament-like proteins that may influence cell shape maintenance were recently identified in *H. pylori* (Waidner et al., 2009).

Biophysical modeling has recently suggested an alternative pathway to generating cell curvature and twist through local alteration of PG crosslink number or length (Huang et al., 2008). Here we present biological evidence supporting this model with the identification of four proteins that function to generate *H. pylori*'s helical shape through alterations in PG crosslinking. We show that these proteins are conserved in other Epsilonproteobacteria as well as curved and helical Gammaproteobacteria, suggesting this approach to generating cell shape may be common among Gram-negative bacteria. We also examine the fitness of nonhelical *H. pylori* mutants in the mouse stomach and find they are deficient despite apparently normal motility in vitro.

RESULTS

A Putative Metallopeptidase, Csd1, Is Required for the Helical Cell Shape of *H. pylori*

To identify genetic determinants of *H. pylori*'s conserved helical cell shape, we visually screened a library of random transposon insertion mutants constructed in strain G27 (Salama et al., 2004) for clones with shape defects. Of 2000 clones screened, nine with altered morphology were selected, including one with curved-rod (vibrioid) rather than helical morphology. Amplification of the DNA sequence flanking the transposon revealed this clone's insertion site was within HPG27_1481 (Figure 1A), a gene annotated as *tagE* due to its homology to a ToxR-activated gene in *Vibrio cholerae* (Kovach et al., 1994). *V. cholerae* contains multiple TagE homologs, and although one has been crystallized and shown to contain a metallopeptidase active site similar to that of the *Staphylococcus aureus* endopeptidase LytM (peptidase family M23; proteins with this domain will be referred to as LytM peptidases for clarity), their function remains unknown (Ragumani et al., 2008). Protein structure queries (Bennett-Lovsey et al., 2008) revealed HPG27_1481 threaded onto the tertiary structures of the crystallized *V. cholerae* TagE protein (*E*-value $3.9E^{-25}$) and *S. aureus* LytM (*E*-value $7.3E^{-23}$). Using these models, we identified conserved LytM active site residues in the HPG27_1481 protein (see below). Targeted deletion of HPG27_1481 coding sequence recapitulated the morphological phenotype of the transposon mutant (Figures 1D and 1E and Figure S1C available online) and was complemented by reintroduction of HPG27_1481 at a distal chromosomal locus, *rdxA*, which is often used for complementation in *H. pylori* (Smeets et al., 2000) (Figures S2B and S2C). Having identified HPG27_1481 as a putative LytM peptidase involved in producing helical versus curved-rod morphology, we named this gene *csd1* (cell shape determinant).

csd1 Is Part of a Three-Gene Locus Required for Helical Cell Morphology

All sequenced *H. pylori* strains encode a second LytM peptidase (HPG27_1482) immediately upstream of *csd1* that is 53% similar and 29% identical to Csd1 (Figure 1A). We designated this gene *csd2* upon discovering its deletion also yielded cells with curved-rod morphology (Figure 1F) and complementation restored helicity (Figure S2C). The hypothetical protein encoded downstream of *csd1* is a homolog of *ccmA* (curved cell morphology, HPG27_1480, Figure 1A), a gene of unknown function shown to be important for determining straight-rod versus curved-rod morphology in *Proteus mirabilis* (Hay et al., 1999). Deletion of *H. pylori ccmA* again resulted in curved-rod morphology (Figure 1G) and could be complemented (Figures S2B and S2C).

Microscopic examination of the three curved-rod mutants suggested slight variations in the degree of cell curvature, with *csd2* the most curved and *ccmA* the least. No helical cells were seen in any of the mutant cell populations. To distinguish whether the mutants had completely lost the ability to form helices or their helical turns had a longer period such that individual cells only appeared curved, we induced cell filamentation with the drug aztreonam, an inhibitor of septal PG synthesis. In comparison with the regular pitch of helical wild-type cells, there

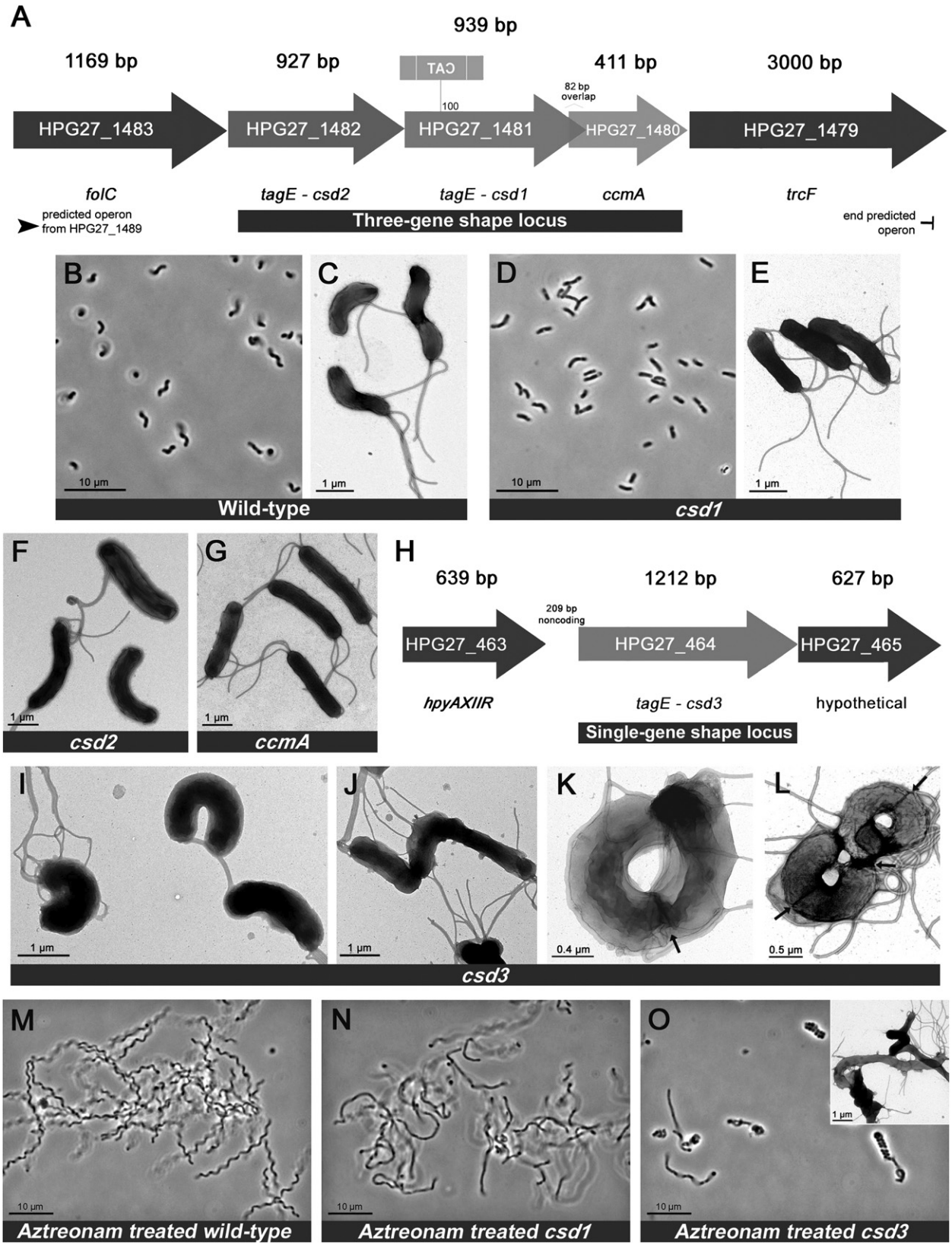
A
939 bp
1169 bp
927 bp
TAG
411 bp
3000 bp
82 bp overlap
100
HPG27_1483
HPG27_1482
HPG27_1481
HPG27_1480
HPG27_1479
folC
tagE - csd2
tagE - csd1
ccmA
trcF
predicted operon from HPG27_1489
Three-gene shape locus
end predicted operon
B
C
D
E
10 μm
1 μm
Wild-type
csd1
F
G
csd2
ccmA
H
639 bp
1212 bp
627 bp
209 bp noncoding
HPG27_463
HPG27_464
HPG27_465
hpyAXIIR
tagE - csd3
hypothetical
Single-gene shape locus
I
J
K
L
0.4 μm
0.5 μm
csd3
M
N
O
Aztreonam treated wild-type
Aztreonam treated csd1
Aztreonam treated csd3

did not appear to be any pattern to the mutants' slight bends and curves (Figures 1M and 1N, Figure S1D, and data not shown). In addition to the loss of helicity, all three were slightly wider than wild-type (7%–14%), but not significantly different in cell length (Figures S2D and S2E). In conclusion, deletion of any single gene in this three-gene locus led to impaired helical twist and gene-specific reductions of curvature.

Loss of *csd3* Results in Variable Curved-Rod Morphologies

All sequenced *H. pylori* strains encode a third LytM peptidase at a separate locus (HPG27_464, Figure 1H) that is 39% similar and 21% identical to Csd1. Deletion of this gene, designated *csd3*, resulted in curved rods with varying degrees of curvature. Although most *csd3* mutant cells appeared highly curved or "c"-shaped (Figure 1I), some had little or no curvature (Figure 1J). Elongated cells (those readying to divide or filamented with aztreonam) appeared as concatenated "c"-shapes that sometimes wound into coils (Figures 1K and 1O, Figure S1E) or figure-eights (Figure 1L). Of 100 cells inspected by transmission electron microscopy (TEM), we observed 17% straight or bent, 53% "c"-shaped, 25% coiled or figure eight, and 5% coccoid. *Csd3* mutant cells were slightly wider (13%) and shorter (10%) than wild-type cells (Figures S2D and S2E), and normal helical morphology was restored with complementation (Figure S2C). In sum, loss of *csd3* resulted in a myriad of highly aberrant cell morphologies stemming from variable curvature and loss of normal helical pitch.

All Four Shape Genes Uniquely Contribute to a Helical Shape-Generating Program

Wild-type cells display a range of morphologies and the differences in shape between our mutant strains were subtle. To further explore functional relationships among these shape genes, we constructed a series of multiple-gene deletion mutants and developed software tools for quantitatively analyzing their morphologies. By capturing images of hundreds of cells and systematically measuring shape parameters, we can rigorously establish differences among strains. Figure S2A illustrates our shape analysis methodology, which consists of collecting high-magnification phase contrast images of each strain and recording each cell's shape as a polygonal outline. The "central axis" of each cell, running from pole to pole, is then determined algorithmically and used to measure cell length, while the degree of cell body curvature is determined directly from the cell outline (excluding the poles) (Lacayo et al., 2007). These morphological parameters clearly delineate wild-type from mutant populations and the subtle differences in the cell body curvature among *csd1*, *csd2*, and *ccmA* mutant populations (Figures 2A and 2B).

We constructed a *csd1csd2* double mutant and a *csd1csd2ccmA* triple mutant by deleting the appropriate coding regions. Visually, the *csd1csd2* mutant's morphology appeared most similar to that of the *csd1* mutant and the *csd1csd2ccmA* mutant's morphology appeared most similar to that of the *ccmA* mutant. The curvature distributions shown in Figure 2C confirmed these observations. Taken together, these results suggest these three genes act in the same pathway to generate helical cell shape.

We next constructed the triple *csd1csd2csd3* mutant and the quadruple *csd1csd2csd3ccmA* mutant. Although the *csd3* mutant population is clearly distinguishable from the other single gene *csd* mutants (Figure 2D), the triple *csd* mutant and quadruple mutant populations overlap completely with the *csd3* mutant, showing the same range of morphological variability and high degree of maximal curvature (Figures 2E and 2F). These findings suggest *csd3* functions in the same or a related shape-generating pathway as *csd1, csd2*, and *ccmA*, but *csd3* may antagonize the activity of the other three genes. Furthermore, whereas each of the four genes is required for generating *H. pylori*'s normal helical shape, none is absolutely required for cell curvature.

Csd Proteins Are Conserved in Epsilonproteobacteria, as well as Vibrioid and Helical Members of the Gammaproteobacteria

Having established an important role for the Csd proteins and CcmA in *H. pylori*'s cell shape, we investigated their conservation in other Epsilonproteobacteria and more broadly throughout the Proteobacteria. Proteins containing a conserved C-terminal LytM peptidase domain are widespread in bacteria, leading us to focus on Csd1 and Csd3 BLAST hits with good sequence alignment over at least 75% of their length and a minimum of 50% total amino acid similarity. Csd1 showed the broadest conservation with a homolog present in most Epsilonproteobacteria and in 14 species representing five different orders within the Gammaproteobacteria, including all members of the Vibrionaceae and *Thiomicrospira crunogena*, a curved-to-helical Gammaproteobacterium (Table S1, Figure 3A). *csd1* is adjacent to *ccmA* in most of the curved and helical species. Some Vibrionaceae genomes contained two well-conserved Csd1 homologs, but each was more closely related to Csd1 than Csd2, suggesting the two Vibrionaceae peptidases arose from a separate duplication or transfer event than that which gave rise to *Helicobacter* Csd1 and Csd2. Indeed, Csd2 homologs were found only in *H. pylori* and *H. hepaticus.* Csd3 homologs, which contain an N-terminal extension not present

Figure 1. *H. pylori* Cell Shape Loci and Their Associated Mutant Morphologies

(A) Three-gene shape locus identified in visual screen. The insertion site of the curved-rod shape mutant's transposon encoding chloramphenicol acetyltransferase (*cat*) in reverse orientation occurred approximately 100 bp into the HPG27_1481 open reading frame.

(B–G) Phase contrast and transmission electron microscopy (TEM) images of wild-type and mutant cells. H) Single-gene shape locus containing *csd3*.

(I–L) TEM images of single *csd3* mutant cells (I and J) and *csd3* mutant cells that are elongated and preparing to divide (K and L, septa indicated by arrows).

(M–O) Phase contrast and TEM images (inset) of wild-type and mutant cells treated with the filamenting drug aztreonam. Strains used: NSH57, LSH13, KGH8, KGH10, LSH112.

See also Figures S1 and S2.

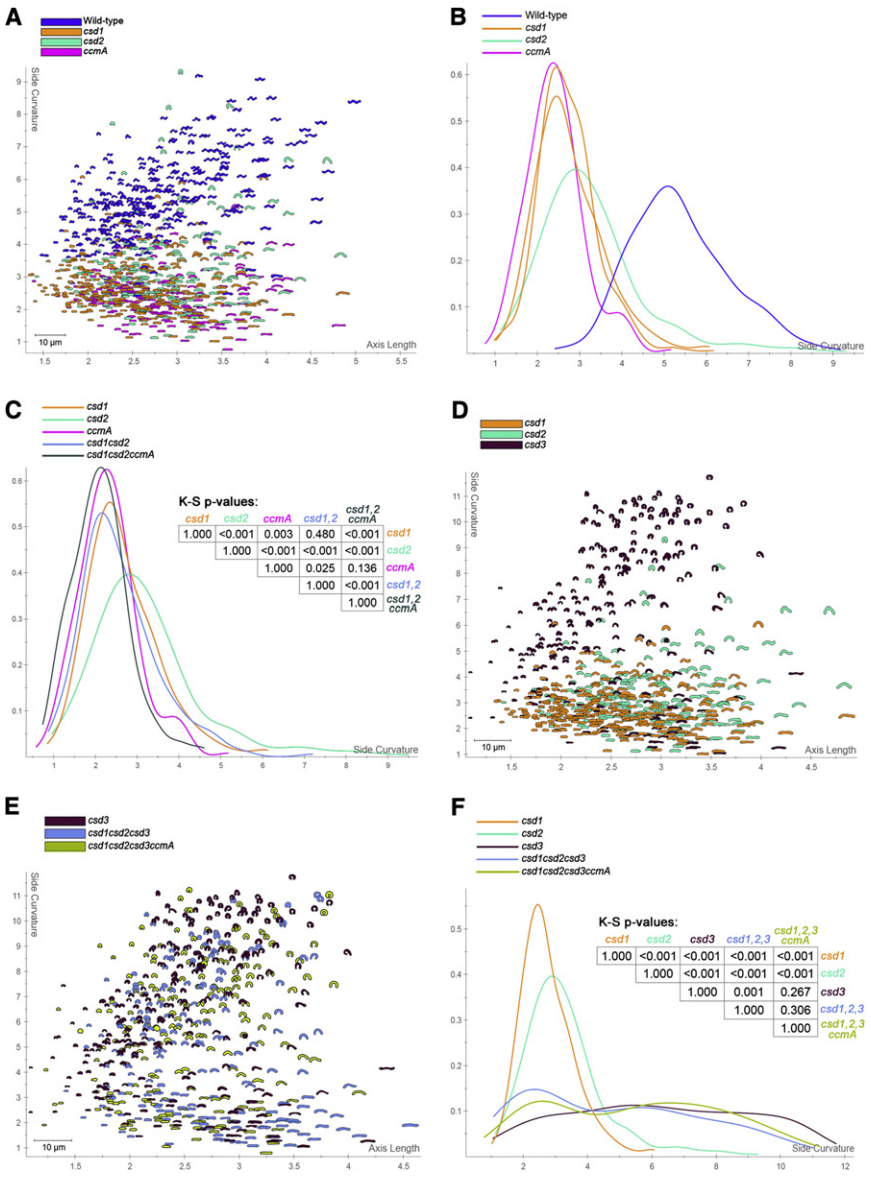

Figure 2. Morphological Characterization of Single and Multiple-Gene Deletion Mutants

(A, D, E) Scatter plots arraying wild-type and/or mutant populations by cell length (*x* axis) and cell curvature (*y* axis). A small proportion (~14%–18%) of cells in mutant strains containing a *csd3* deletion were so highly curved as to erroneously appear coccoid after image processing; these cells were manually removed from the analysis.

(B, C, F) Smooth histograms displaying population cell curvature (*x* axis) as a density function (*y* axis) and p-values from bootstrapped Kolmogorov–Smirnov statistical comparisons. Replicate *csd1* mutant populations used to define the null distribution for statistical comparisons of curved-rod strains are shown in panel B. Strains used: NSH57, LSH13, KGH8, KGH10, LSH112, LSH129, LSH130, LSH136, LSH143.

in Csd1 and Csd2, were well conserved in all five strains of *Helicobacter* and throughout the Epsilonproteobacteria, but were not identified in other classes of Proteobacteria.

All the *csd1* and *csd3* homologs identified preserve conserved residues predicted to function in catalysis (see the stars in Figure 3A). Mutation of one such residue, H250A (arrow in Figure 3A), in the endogenous *csd1* gene resulted in a slightly curved-rod morphology indistinguishable from the null allele (Figures 3B and 3C and Figure S3A). We attempted to complement the shape phenotype of the *csd1* null mutant with the *C. jejuni* and *V. cholerae* homologs. Unlike the *csd1* gene from *H. pylori* (Figure S2B), neither homolog fully restored normal shape (Figures 3C and 3D), but occasional cells displayed additional bends or an S-like shape never seen in the null allele strain (Figures 3C and 3D, Figures S3B and S3C). Based on the heterogeneity of the shapes of the cross-species complementation strains it is difficult to say whether Csd homologs contribute to cell morphology in other Proteobacteria, but in *H. pylori*, peptidase activity is required for Csd shape-generating function.

Global Peptidoglycan Analyses Suggest Helical Cell Shape Is Specified by Peptidoglycan Peptide Crosslinking

The presence of LytM domains in the Csd proteins suggests they are PG endopeptidases or carboxypeptidases. We first established that the cell shape changes observed in the *csd* mutants coincided with changes in the shape of isolated mutant PG sacculi (Figures 4A–4F). We observed that sacculi from *H. pylori* behaved differently than those from *E. coli* or *C. crescentus* in that they contrasted very poorly with uranyl acetate for visualization by electron microscopy (Figures 4B and 4E). Hence, the *H. pylori* sacculi required detection by negative staining (Figures 4C, 4D, and 4F). The reason for this difference is not known, but *H. pylori* PG may have wider pores and fewer sites for binding of heavy metal ions than PG from other species. The isolated sacculi nevertheless displayed the shape of intact cells: helical rod for wild-type (Figures 4A–4C) and rods with varying curvature for *csd1* and *csd3* mutants (Figures 4D–4F). Thus, as in straight and curved-rod bacteria with a PG cell wall, the structural determinant of cell shape in *H. pylori* is the PG sacculus.

We then analyzed the global muropeptide composition (described in Figure 4G and Figure S4A) of *csd1*, *csd2*, and *csd3* null mutants and the *csd1*^{H250A} point mutant compared with wild-type, as well as the *csd1* and *csd3* complemented strains. Although glycan strand length was unchanged, the content of the peptide side chains in each mutant was

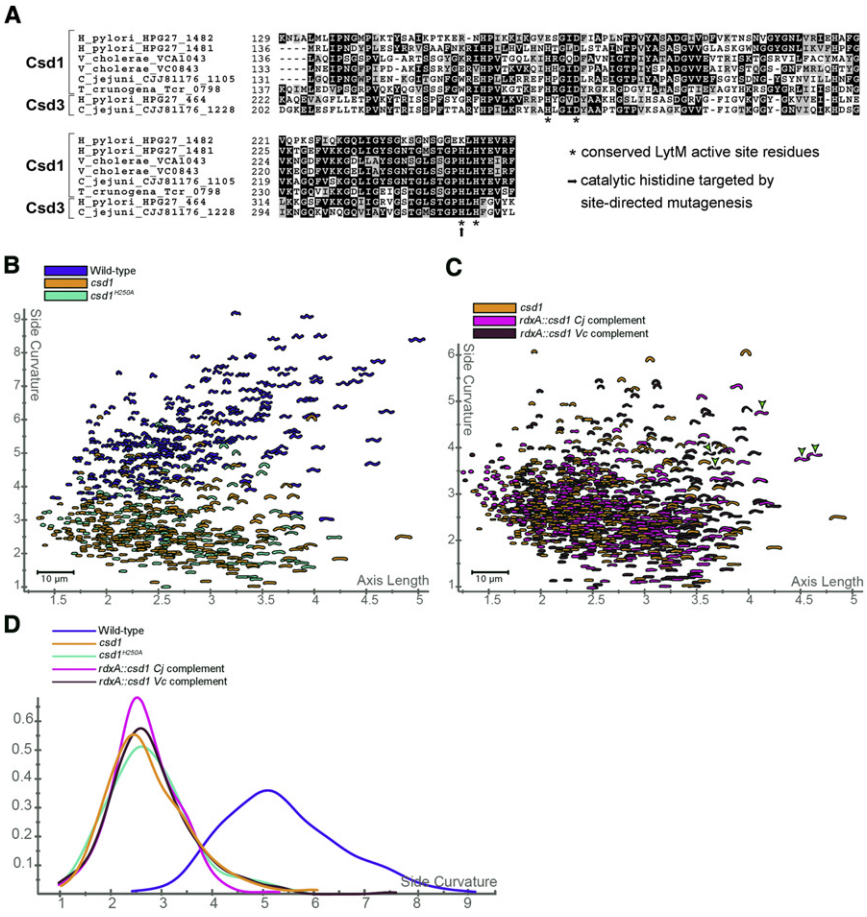

Figure 3. Conservation of Csd Proteins in Epsilonproteobacteria and Gammaproteobacteria

(A) Multisequence alignment of LytM domains in *H. pylori*, *C. jejuni*, *V. cholerae*, and *T. crunogena* Csd1 and Csd3 protein homologs listed by species and locus tag. Stars indicate positions of conserved LytM active site motifs HXXXD and HXH (Ragumani et al., 2008). The arrow shows histitidine residue mutated to alanine (H250A).

(B) Distribution of wild-type, *csd1* null, and *csd1*^{H250A} point mutant populations.

(C) Distribution of *csd1* null population compared to cross-species complementation of *csd1* from *C. jejuni* (*Cj*) and *V. cholerae* (*Vc*). Semi-helical shapes rarely observed in cross-species complementation strains and never in the parent *csd1* null are marked with green arrowheads.

(D) Smooth histograms showing the side curvature distribution for the above populations. All mutant and complement populations are significantly different from wild-type (bootstrapped K–S p value < 0.00001), but indistinguishable from *csd1* null ($p > 0.9$). Strains used: NSH57, LSH13, LSH153, NSH142, NSH144.

See also Table S1 and Figure S3.

significantly altered from wild-type (Table 1, Figure S4B, and Table S2). The most dramatic change was a 26%–49% increase in tetrapentapeptide crosslinked dimers, which coincided with an 8%–33% decrease in tetrapeptide monomers in all mutants. In the two complemented strains these muropeptides were unchanged from wild-type levels or the inverse change was observed. The latter effect is likely due to higher expression levels from the *rdxA* locus relative to the native loci (quantitative RT-PCR data not shown). For these changes to be perfectly balanced, we would have expected a decrease in pentapeptide monomers in the mutants, but this was only observed in the *csd2* mutant. This discrepancy may result from trimming of penta-peptide monomers by other endopeptidases or carboxypeptidases, yielding tetra-, tri-, and/or dipeptide monomers. Accordingly, we observed decreases of greater than 10% in the tripeptide monomer content of the *csd1*^{H250A}, *csd2,* and *csd3* mutants, and the dipeptide monomer content of the *csd1* null mutant; these changes were reversed in the *csd1* and *csd3* complemented strains. We also tested the profile of the *ccmA* mutant and found that it too contained significant alterations in its muropeptide content relative to wild-type, including the same increase in tetrapentapeptide crosslinked dimers and decrease in tetrapeptide monomers as the *csd* mutants. Because CcmA does not contain any recognizable peptidase motif, it may function through interaction with Csd peptidases. Together these data suggest the Csd proteins could be endopeptidases that cleave tetrapentapeptide PG crosslinks.

For *csd1*, *csd2*, and *ccmA*, the increases in tetrapentapeptide crosslinking correlated with a loss of helical twist and cell curvature. The *csd3* mutant also lost normal helical twist, but many cells displayed a higher degree of cell curvature. The *csd3* mutant exhibited other significant changes in crosslinked muropeptide content; both tetratetrapeptide and tetratripeptide dimers were decreased by over 30% and restored with complementation. It is thus possible that Csd3 also exhibits a carboxypeptidase activity, converting tetrapentapeptide crosslinks into tetratetrapeptide crosslinks, which are further degraded to tetratripeptide crosslinks by another carboxypeptidase. The highly curved morphology observed for *csd3* may result from the loss of tetratetrapeptide and tetratripeptide crosslinks observed uniquely in this mutant's PG. In sum, each of our mutants exhibited changes in glycan strand connectivity associated with variation in cell curvature and twist.

Changes in the *csd* Mutants' Cell Shape and Cell Wall Composition Minimally Affect Motility and Do Not Alter Growth or Sensitivity to Stomach Environment Stresses

All the mutants described here were normally flagellated and motile in broth (data not shown), but the corkscrew model for helical shape posits that they should be impaired for motility in gel-like media. We characterized their ability to swim directionally in a soft agar motility assay, and found each performed as well or better than wild-type with the exception of the *csd3*

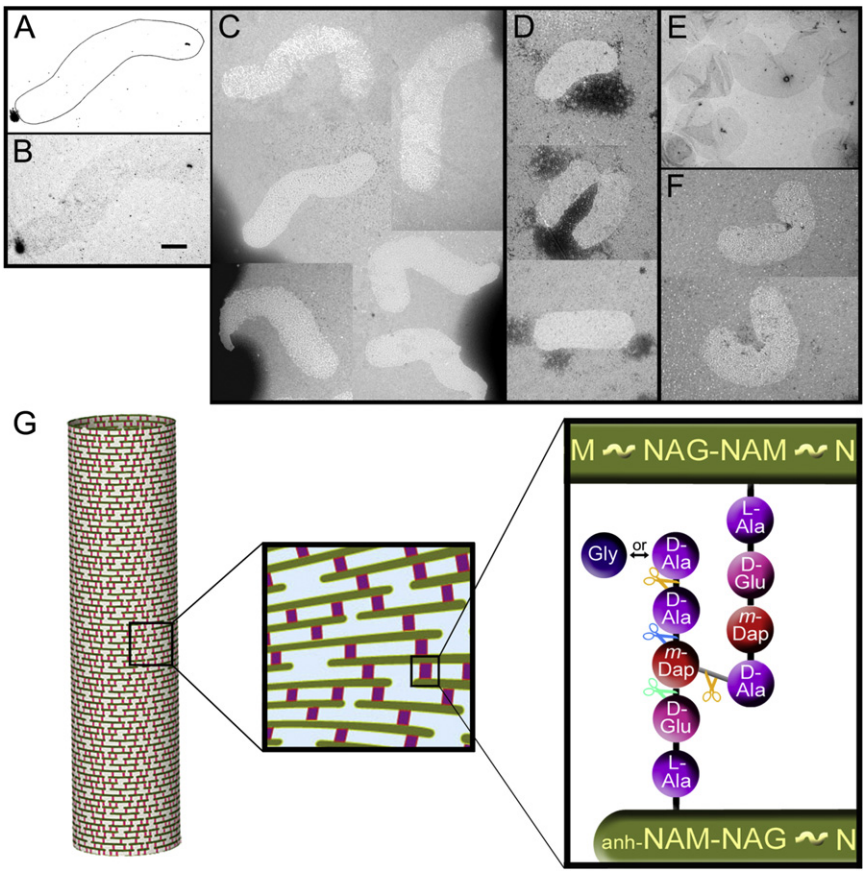

Figure 4. Transmission Electron Microscopy Images and Schematic Illustration of Peptidoglycan Sacculi

(A and B) Schematic drawing (A) outlining the poorly visible uranyl acetate-stained wild-type *H. pylori* sacculus depicted in the image directly below (B).

(C) Negatively stained wild-type *H. pylori* sacculi. Morphological variability among the sacculi is a product of their two-dimensional flattening during fixation on the grid, but the apparent wave form of the sacculi approximates the helical morphology of intact cells as observed by TEM (Figure 1C).

(D–F). *csd1* (D) and *csd3* (E–F) mutant sacculi illustrating their slightly (*csd1*) or strongly (*csd3*) curved-rod morphologies, as seen in the intact cells (Figure 1E and 1I). Panel E shows sacculi contrasted with uranyl acetate, others are negatively stained. The scale bar (0.5 μm) applies to all images. Strains used: LSH108, LSH115, LSH119.

(G) Schematic illustration of PG mesh structure that envelops the cell and is composed of glycan strands (green) interconnected by peptide crosslinks (red). Glycan consists of repeating *N*-acetylglucosamine (NAG or Glc*N*Ac)–*N*-acetylmuramic acid (NAM or Mur*N*Ac) disaccharides with a 1,6–anhydro ring (anh) on NAM sugars at strand termini. Peptide chains extend from each NAM. Shown is the tetra-pentapeptide muropeptide with the peptide crosslink highlighted in gray. *m*-Dap refers to *meso*-diaminopimelic acid. Peptide bonds marked with orange scissors may be hydrolyzed by DD-endopeptidases (cleaving DD-peptide bridges) or DD-carboxypeptidases (producing tetrapeptide), those marked with blue scissors may be hydrolyzed by LD-endopeptidases (producing tripeptide), and those marked by green scissors may be hydrolyzed by DL-endopeptidases or DL-carboxypeptidases (producing dipeptide). Altogether, these modification activities give rise the other muropeptides depicted in Figure S4A.

mutant, which formed smaller halos (Figure 5A). This motility defect might be explained by the observation that the coiled and nearly coiled *csd3* mutant cells swam in tight circles in broth, whereas cells with less curvature displayed normal directional motility. To further explore a relationship between motility and loss of normal helical twist, we used video microscopy to compare the swimming velocity of wild-type and *csd1* mutant cells in media with and without methylcellulose. We observed the wild-type swimming 22.0 μm/s on average in both media (broth 22.0 ± 13.7 μm/s, 0.5% methylcellulose 22.3 ± 15.8 μm/s, mean of 20 cells ± standard deviation [SD]) and the *csd1* mutant swimming 16 μm/s on average in both media (regular broth 15.8 ± 8.9 μm/s, 0.5% methylcellulose 15.9 ± 8.5 μm/s, mean of 20–21 cells ± SD). Thus, the curved-rod mutant was not hampered in swimming velocity compared with wild-type in either broth or viscous methylcellulose solution (two-sided Student's t tests, $p > 0.05$).

Each of the mutant strains grew as well as wild-type through log and into stationary phase in single-strain cultures and during 72 hr of log phase growth in coculture with wild-type (Figures S5A–S5H). Whereas *H. pylori* in log phase display helical morphology, the cells undergo a shape transition to a nonculturable coccoid form during prolonged culture in stationary phase (Benaissa et al., 1996; Andersen and Rasmussen, 2009). All four mutants were capable of fully transforming into nonculturable coccoids, but *csd3* mutants were slightly delayed in the timing of the process (Figure S5I and data not shown).

Because all the mutants exhibited similar alterations in their peptidoglycan that might alter the integrity of the cell wall, we subjected *csd1* cells to stresses *H. pylori* encounters in the stomach: antimicrobial peptides, acid, and medically administered amoxicillin, an antimicrobial that targets the cell wall. The *csd1* mutant survived as well as the wld-type upon exposure to the antimicrobial peptide polymyxin and low pH (Figures 5B and 5C). We also found the *csd1* strain was slightly more resistant to amoxicillin than wild-type (minimum inhibitory concentration: *csd1* 0.079 ± 0.020 μg/ml, wild-type 0.045 ± 0.014 μg/ml, mean ± SD). Collectively, these data show that the cell wall changes produced in these mutants do not appreciably alter cell wall integrity.

Curved-Rod *H. pylori* Mutants Are Outcompeted by Helical Wild-Type Cells in the Mouse Stomach

Although we observed no apparent enhancement of motility mediated by helical shape, we wondered whether helical cell shape might have some other selective advantage in the gastric niche.

Table 1. Summary of Global Peptidoglycan Composition in Mutant and Complemented Strains

	Area—% of Each Muropeptide[a]								
Muropeptide Species and Structural Features	Wild-Type	*csd1*	*csd1 rdxA:: csd1*	*csd3*	*csd3 rdxA:: csd3*	*csd2*	*ccmA*	Wild-Type[b]	*csd1*^{H250A} [b]
Monomers (total)	56.97	52.84	54.16	50.54	57.29	51.03	51.55	53.06	51.04
Monomer di	1.90	1.65	**2.98**	2.14	**3.38**	2.21	**3.00**	2.06	2.24
Monomer tri	4.87	4.57	3.96	**3.35**	5.13	4.17	3.99	4.37	3.65
Monomer tetra	9.35	**7.11**	9.59	**6.31**	**11.72**	**7.12**	7.82	8.93	8.22
Monomer penta	40.85	39.50	37.63	38.75	37.06	37.52	36.74	37.69	36.94
Monomers anhydro	2.05	**1.43**	**1.61**	**1.48**	**1.62**	**1.55**	**1.49**	1.41	1.32
Dimers (total)	38.01	43.79	40.20	41.64	37.50	43.42	42.68	39.18	44.74
Dimers tetra-tri	4.72	3.83	4.84	**3.18**	4.78	4.54	4.44	4.33	3.80
Dimers tetra-tetra	13.58	13.98	15.42	**9.17**	15.29	14.10	15.16	15.07	16.05
Dimers tetra-penta[c]	19.71	**25.98**	19.94	**29.30**	17.43	**24.78**	23.08	19.77	**24.89**
Dimers anhydro	12.67	13.29	**15.58**	14.47	**15.25**	14.42	13.95	16.32	17.43
Dipeptides (total)	1.90	1.65	**2.98**	2.14	**3.38**	2.21	**3.00**	2.06	2.24
Tripeptides (total)	7.23	6.49	6.38	**4.94**	7.52	6.44	6.21	6.54	5.54
Tetrapeptides (total)	35.14	35.99	37.40	31.71	38.12	35.88	36.74	36.06	38.61
Pentapeptides (total)	50.70	52.50	47.61	53.40	45.78	49.91	48.28	47.57	49.39
Glycine (total)	5.51	6.52	4.83	**7.30**	5.03	6.35	5.95	4.30	**5.88**
Glycine monomer	4.48	5.06	3.97	**5.65**	4.40	4.99	4.70	3.51	**4.57**
Glycine dimer	2.05	**2.93**	1.72	**3.30**	**1.26**	**2.72**	**2.51**	1.57	**2.63**
% of peptides in crosslinks	38.01	43.79	40.20	41.64	37.50	43.42	42.68	39.18	44.74
Mean glycan chain length	11.93	12.38	10.64	11.47	10.82	11.42	11.82	10.45	9.97
% of anhydro termini at crosslinks	75.52	82.25	82.90	83.01	82.45	82.31	82.45	85.27	86.85

[a] Percentages calculated as per (Glauner et al., 1988). Underlined, value differs by more than 10% from that of wild-type; underlined and bold, value differs by more than 20% from that of wild-type. The following strains were used: LSH108, LSH110, LSH115, LSH119, LSH121, and LSH126 (experiment 1) and LSH100 and LSH154 (experiment 2).
[b] Analysis performed in a separate experiment.
[c] Inclusive of tetra-penta, tetra-penta(Gly5), and tetra-penta anhydro peaks from Table S2.

We thus tested the fitness of the *csd1*, *csd2*, and *ccmA* mutants alongside wild-type in a mouse stomach colonization assay. All three mutants were strongly outcompeted by wild-type at 1 week, with mutant bacteria recovered from only a few mice, and the *csd1* phenotype was complemented (Figures 5D and 5E). In order to determine whether the cell shape mutants were capable of colonizing and surviving in the stomach in the absence of wild-type bacteria, we infected mice with the *csd1* mutant alone. Although only two of the five *csd1*-infected mice were colonized (compared with four of five mice infected with wild-type), both were colonized to wild-type levels (Figure 5F). These data indicate that normal helical shape and/or peptidoglycan crosslinking promotes efficient stomach colonization by *H. pylori*.

DISCUSSION

Here, we have identified four genes (*csd1–3* and *ccmA*) that each uniquely affect bacterial cell morphogenesis but not septation or growth of the helical bacterium *H. pylori*. All four proteins influence peptide crosslinking within the peptidoglycan sacculus and three encode LytM peptidase homologs, suggesting they may be endopeptidases and/or carboxypeptidases that directly hydrolyze PG crosslinks or otherwise modify PG. The total extent of peptide crosslinking in the mutants did not change by more than 15%, but the abundance of specific crosslinked muropeptides changed as much as 50%. This, combined with the observation that isolated mutant sacculi displayed the same alterations in shape as intact cells, suggests that even subtle perturbations of PG crosslinking are sufficient to disrupt helical cell shape in *H. pylori.*

To our knowledge, an association between PG crosslinking and cell curvature or twist has not previously been established in a biological system. Rod-shaped *C. crescentus creS* mutants did not show alterations in PG crosslinking (Cabeen et al., 2009). Also, studies of the straight-rod bacterium *E. coli* found no obvious change in cell shape upon deletion of any of the low-molecular-weight PBP endopeptidases and carboxypeptidases, either alone or in combinations that left only DacD and a few penicillin-insensitive peptidases active (Denome et al., 1999). Varma et al. induced spirillum-like morphology in *E. coli* by inhibiting FtsZ in a mutant lacking PBP5 and PBP7, the latter a DD-endopeptidase that hydrolyzes tetrapentapeptide crosslinks (Varma and Young, 2004). However, the authors

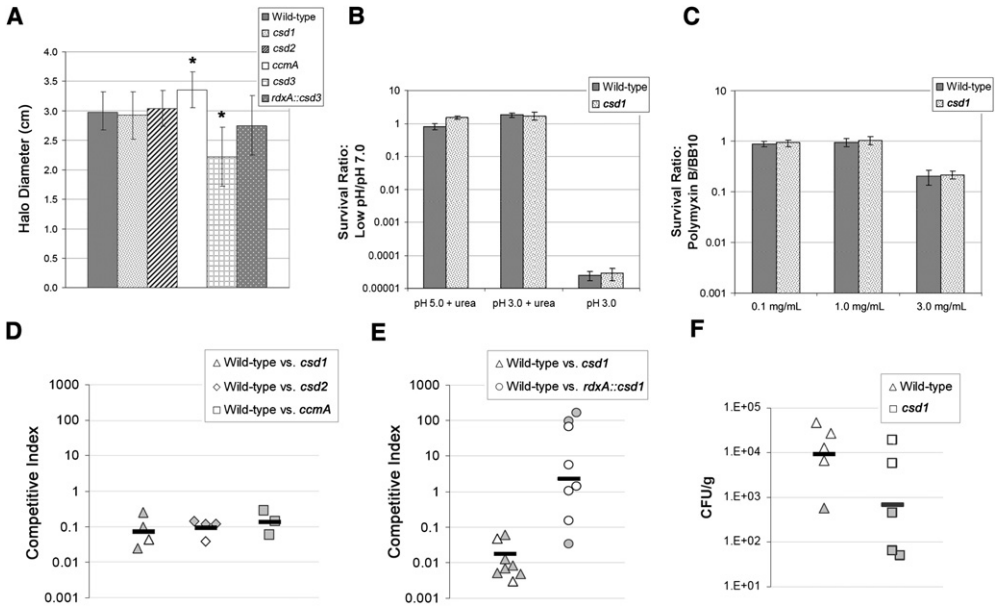

Figure 5. Phenotypes of Nonhelical Mutants and Complemented Strains in the Mouse Stomach and Related In Vitro Conditions

Complementation strains have the native locus disrupted by deletion and insertion of *cat* and the indicated gene expressed from the *rdxA* locus.

(A) Motility phenotype of mutant and complemented strains in soft agar (mean halo diameter inclusive of two or three independent experiments totaling 40–50 stabs per strain ± SD in 0.3% soft agar after four days). Stars indicate significant difference from wild-type ($p < 0.05$, ANOVA with Bonferroni correction).

(B and C) Survival in stomach stress conditions from two independent experiments, each with four replicates per strain and condition (mean survival ratio ± SEM).

(D and E) One week C57BL/6 mouse competition data. Each data point represents a single mouse. Data are plotted as a competitive index: [CFU/ml$_{MUT}$:CFU/ml$_{WT}$ stomach output]/[CFU/ml$_{MUT}$:CFU/ml$_{WT}$ inoculum]. Filled points indicate mice from which only one strain was recovered, causing the competitive index to be driven largely by the load of the infecting (wild-type) strain. Mean loads were 560 CFU/stomach, range 100-1050 (D) and 6600, range 2100-19100 (E). Black bars are the geometric mean.

(F) One week C57BL/6 single strain colonization data. Each data point represents the load (CFU/g) from a single mouse. Filled points indicate mice from which no bacteria were recovered and are plotted at the detection limit. Black bars are the geometric mean. Strains used: A, D, and F) LSH100, LSH113, LSH141, LSH142, LSH119, LSH126; B–C) NSH57, LSH13; E) NSH57, LSH11, LSH102.

See also Figure S5 and Movie S1.

did not report whether PG crosslinking was altered in these cells, and the mechanism responsible for this observation remains unknown.

Recent biophysical modeling suggested that hydrolysis of PG crosslinks on the outer edge of the cell can induce cell curvature and that a shortening of the length of the crosslinks along a helical path might induce helical morphology (Huang et al., 2008). As *H. pylori* PG lacks the shorter type of crosslink found in some bacteria, (LD)-*m*Dap–*m*Dap (Costa et al., 1999), we propose that this organism could achieve both curvature and twist by hydrolyzing PG crosslinks at specific points along the cell. Curving the cell body might be achieved by hydrolyzing crosslinks, and thus relaxing the connectivity of the rigid glycan strands, along a straight axis on the outer curvature (Figure 6, blue). Twist may be achieved by shifting this axis diagonally (Figure 6, pink) and/or hydrolyzing crosslinks near the inflection point of the curve (Figure 6, yellow), enabling the glycan hoops in that region to slip a little such that the ends of the curve are off-set and a regular helical pitch is defined. This model implies PG hydrolytic activities are precisely localized, perhaps along multiple axes. We have shown that *H. pylori* indeed expresses multiple proteins that are each required for helical shape maintenance and result in unique morphological perturbations upon deletion. This coupled with the fact that at least three of the proteins seem to be redundant in the major PG biochemical alterations they cause supports the theory that these proteins may be spatially regulated. However, the task of positioning Csd/CcmA activities would likely require the involvement of other proteins, perhaps cytoskeletal proteins such as MreB, FtsZ, or CreS, and these mechanisms remain to be elucidated. Another hypothesis to be tested is whether the morphogenic effect of changes in PG crosslinking is amplified by the induction of gradients in PG synthesis rates as a direct result of crosslink hydrolysis (i.e., stressing of the remaining transpeptide bonds could locally facilitate PG synthesis).

Little is known about the structural and functional diversity of LytM peptidases aside from the fact they are multidomain proteins with a four-stranded antiparallel β sheet active site in the C-terminal half of the sequence (Odintsov et al., 2004; Ragumani et al., 2008). Some Gram-negative proteins, such as NlpD and the crystallized *V. cholerae* protein VCO503, contain PG-binding LysM domains in the N-terminal half of the protein (Ragumani et al., 2008; Uehara et al., 2009), which could be important for substrate recognition or localization. A recent study inactivated all four of the *E. coli* LytM peptidases, EnvC, NlpD, YgeR, and YebA, finding that the *envC* mutant had a slight

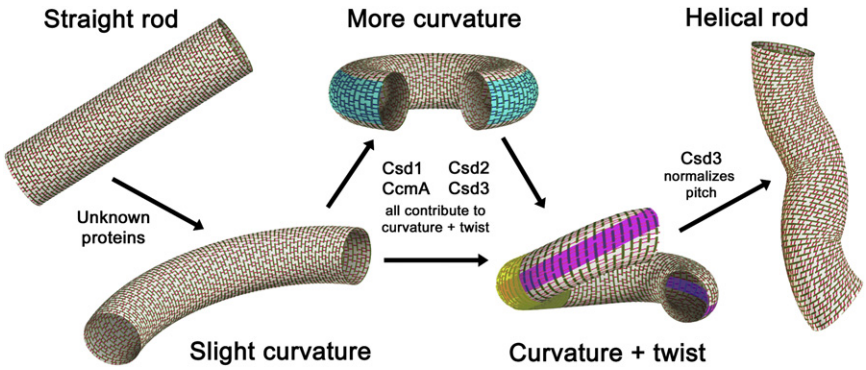

Figure 6. Model of How *H. pylori*'s Peptidoglycan Sacculus Forms Helical Curvature and Twist

Glycan strands are green and peptide crosslinks red. Blue, pink, and yellow highlights indicate possible zones where relaxation of peptide crosslinking may contribute to the indicated curved and twisting morphologies.

septation defect, which became more severe when *nlpD* was also deleted (Uehara et al., 2009). The global PG composition of all of these mutants was unchanged from wild-type and no precise biochemical activity has yet been assigned to any Gram-negative LytM peptidase.

Our analyses of the *csd* null and point mutants' total muropeptide composition indicated that each protein contributes to the hydrolysis of *m*Dap–D-Ala crosslinks and is thus possibly a DD-endopeptidase. Alternatively, the Csd proteins may activate other endopeptidases, resulting in the observed changes in muropeptide profile. The *csd3* mutant was unique in that it showed ~30% decreases in tetratetrapeptide and tetratripeptide crosslinking in addition to the 20%–50% increase in tetrapentapeptide crosslinking evident in all of the mutants. Thus, Csd3 may have multiple activities or may influence the activities of other endopeptidases and carboxypeptidases. The additional relaxation of PG crosslinking in the *csd3* mutant may also explain why all of the mutant strains in which *csd3* was deleted displayed high degrees of curvature. CcmA bears no sequence or structural homology to any known enzyme, yet apparently it also is important for tetrapentapeptide hydrolytic activity. CcmA is peripherally associated to the inner membrane in *P. mirabilis* (Hay et al., 1999) and may exert its function by interacting with the Csd proteins, providing stabilization and/or localization.

Csd1, Csd3, and CcmA are well-conserved throughout the Epsilonproteobacteria, though Csd1 and CcmA homologs were not identified in all species with curved or helical morphologies. Expression of putative *csd1* homologs from the Epsilonproteobacterium *C. jejuni* and the Gammaproteobacterium *V. cholerae* in a *csd1* null background appeared to restore some curvature and helical twist in a small subpopulation of cells, supporting a similar function for these proteins. The lack of robust cross-species complementation may result from poor expression, inappropriate localization, or inefficient interactions with the other Csd and CcmA proteins.

The *csd* and *ccmA* mutants' loss of helicity allowed us to begin to explore the functional role of helical shape in *H. pylori*. Flagellar-based motility is absolutely required for *H. pylori* infection (Eaton et al., 1996), and helical shape was proposed to allow the bacteria to escape the acidic stomach lumen by boring into the gastric mucus like a screw through a cork (Montecucco and Rappuoli, 2001). Our observations question the model that helical shape is required for *H. pylori* motility in gel-like media. Another study has also challenged this dogma by demonstrating urease activity dependent reduction in the viscoelasticity of gastric mucus from the gel-like state at low pH to a solution state at more neutral pH (Celli et al., 2009). In spite of their apparently normal motility, three cell shape mutants were each attenuated for stomach colonization in our mouse infection model. We further showed that the increase in tetrapentapeptide crosslinking observed in *csd* and *ccmA* mutant PG did not lead to an obvious weakening of the cell wall to environmental stresses encountered in the stomach. We thus provide evidence that helical shape or some other PG-related property is required for robust stomach colonization by *H. pylori*, though perhaps not through enhancement of motility.

In this work, we have established *H. pylori* as an excellent model to elucidate molecular determinants of helical cell shape in the Proteobacteria and the selective role of shape during host colonization. Our discovery of a family of LytM peptidase homologs required for efficient stomach colonization by *H. pylori* suggests new targets for antimicrobial therapy that may have efficacy in other pathogens that utilize these proteins, including *Vibrio* and *Campylobacter* species.

EXPERIMENTAL PROCEDURES

Bacterial Strains and Growth

Strains used are described in the Extended Experimental Procedures strain table. *H. pylori* were grown on horse blood (HB) agar plates (Humbert and Salama, 2008) or in Brucella broth (BD Biosciences) containing 10% fetal bovine serum (Hyclone) but no antimicrobials (BB10). Cultures were incubated microaerobically at 37°C in a gas pack jar containing a CampyGen sachet (Oxoid) or in an incubator equilibrated with 14% CO_2 and 86% air. For resistance marker selection, HB plates were supplemented with 15 μg/ml chloramphenicol, 25 μg/ml kanamycin, 36 μg/ml metronidazole, or 60 mg/ml sucrose. For culturing bacteria from mouse stomachs, 200 μg/ml bacitracin was added to eliminate normal mouse microbiota growth. Cell filamentation was induced by diluting overnight liquid cultures to 0.2 optical density at 600 nm (OD_{600}) into BB10 containing 2 μg/ml aztreonam and shaking for 4–9 hr. For plasmid selection and maintenance in *E. coli*, LB agar or broth was supplemented with 30 μg/ml kanamycin or 100 μg/ml ampicillin.

Phase Contrast and TEM Microscopy of *H. pylori* Cells

For phase contrast microscopy, cells were grown in shaken liquid culture to mid-log phase (OD_{600} 0.2–1.0), fixed in a 4% paraformaldehyde/phosphate-buffered saline (PBS) solution containing 10% glycerol, and mounted on glass slides. Cells were imaged with a Nikon TE 200 microscope equipped with a 100× oil-immersion objective and Nikon CoolSNAP HQ CCD camera controlled by MetaMorph software (MDS Analytical Technologies). TEM was

performed as described (Lowenthal et al., 2009). Image cropping and brightness/contrast adjustments were made using Adobe Photoshop Elements 3.0.

Preparation of PG and Analysis of Muropeptides

H. pylori cells were expanded daily on HB plates lacking antimicrobials to maintain log-phase growth and obtain 100–500 OD_{600} per strain. Cells were collected with sterile polyester swabs, suspended in 6 ml chilled PBS, and lysed by dropwise addition to 6 ml boiling 8% SDS. PG was prepared from cell lysate as described (Glauner et al., 1988; Costa et al., 1999). Muropeptides were released from PG by the muramidase Cellosyl (Hoechst, Frankfurt am Main, Germany), reduced by sodium borohydride, and separated on a 250 × 4.6 mm 3 μm Prontosil 120-3-C18 AQ reverse-phase column (Bischoff, Leonberg, Germany) as described (Glauner et al., 1988). The eluted muropeptides were detected by their absorbance at 205 nm. The muropeptide profile of the wild-type was similar to the published profile of *Helicobacter* muropeptides (Costa et al., 1999), allowing unambiguous assignment of known muropeptide structures to the peaks detected.

Visualization of Sacculi by TEM

Sacculi were immobilized for 15 min on glow-discharged carbon-pioloform coated copper grids (400 mesh). Excess liquid was removed onto filter paper and the grids air-dried (de Pedro et al., 1997). Grids were then incubated with 1%–2% uranyl acetate for 1 min, briefly washed with water, and air-dried. Because uranyl acetate treatment gave poor contrast for *H. pylori* sacculi, samples were also visualized by negative staining. A drop of the sacculi suspension was mixed with a drop of staining solution (3% phosphotungstic acid adjusted to pH 7 with potassium hydroxide prior to use) and added to the same grids. After 30 s the excess liquid was removed and the grid air-dried. Samples were examined on a Philips CM 100 Compustage (FEI) transmission electron microscope and digital images collected using an AMT CCD camera (Deben).

Motility, Growth, and Stress Testing

Soft agar motility experiments were performed as described (Lowenthal et al., 2009). For velocity measurements, cells at 0.2 OD_{600} were mixed with an equal volume BB5 with or without 1% methylcellulose and imaged on a hanging drop slide with a 40× objective at 100 ms intervals using phase contrast as described above. Cells were tracked using the ImageJ Manual Tracker (Rasband, 2009) and curvilinear velocity calculations performed with Intercooled Stata 10.0 (StataCorp). Growth and stress testing was accomplished using 100–200 μl BB10 minicultures grown in a 96-well plate. For growth experiments, liquid cultures were grown overnight to $OD_{600} < 1$ and diluted to 0.005 OD_{600}/ml (0.0025 OD_{600}/ml for each strain in coculture experiments). At desired intervals cell aliquots were diluted serially and plated to nonselective and (for coculture experiments) selective HB plates to enumerate total and mutant CFUs. For pH and polymyxin stress testing, 1×10^8 cells from overnight cultures were added to pH-adjusted BB10 or BB10 containing 0.1–3.0 mg/ml polymyxin, incubated for 1 hr, and plated to HB plates. Amoxicillin sensitivity was determined by plating 200 μl overnight culture on HB plates lacking antimicrobials and applying E-test strips (AB Biodisk). Plates were incubated for 2–3 days and read according to the manufacturer's instructions.

Mouse Colonization

Female C57BL/6 mice 24–28 days old and certified free of endogenous *Helicobacter* were obtained from Charles River Laboratories. Mice were housed and infected as described (Amundsen et al., 2008) using 5×10^7 cells/strain in the inocula for competition experiments and 1×10^8 cells in the inocula for single-strain experiments. The whole stomach was homogenized in 1 ml BB10 and dilutions were plated to nonselective and selective (for competition experiments) HB plates to enumerate total and mutant bacteria. If no mutant bacteria were recovered we set the number of colonies on the lowest dilution plated to 1. All studies were done under practices and procedures of Animal Biosafety Level 2. The facility is fully accredited by the Association for Assessment and Accreditation of Laboratory Animal Care, International, and all activities were approved by the FHCRC Institutional Animal Care and Use Committee.

Quantitative Morphological and Bioinformatic Analyses

A detailed description of these methods is provided in the Extended Experimental Procedures.

SUPPLEMENTAL INFORMATION

Supplemental Information includes Extended Experimental Procedures, five figures, three tables, and one movie and can be found with this article online at doi:10.1016/j.cell.2010.03.046.

ACKNOWLEDGMENTS

This work was supported by NIH grants AI054423 and AI082026 (N.R.S.), a National Science Foundation Graduate Research Fellowship (L.K.S.), and grants from the Biotechnology and Biological Sciences Research Council (grant No. BB/F001231/1) and the European Commission (EUR-INTAFAR project) (W.V.). The contents are solely the responsibility of the authors and do not necessarily represent the official views of these funding agencies. We thank J. Fero, C. Tung, G. Cromie, S. Talarico, B. Stoddard, and D. Vollmer for technical assistance and consultation, P. Born for peptidoglycan analysis, R. Burmeister for graphic design, E. Gaynor and S. Miller for strains, and B. Schneider and staff (FHCRC Electron Microscopy Shared Resource), as well as V. Thompson and T. Davies (Newcastle University Electron Microscopy Research Service), for assistance with TEM.

Received: October 21, 2009
Revised: January 29, 2010
Accepted: March 19, 2010
Published: May 27, 2010

REFERENCES

Alyahya, S.A., Alexander, R., Costa, T., Henriques, A.O., Emonet, T., and Jacobs-Wagner, C. (2009). RodZ, a component of the bacterial core morphogenic apparatus. Proc. Natl. Acad. Sci. USA *106*, 1239–1244.

Amundsen, S.K., Fero, J., Hansen, L.M., Cromie, G.A., Solnick, J.V., Smith, G.R., and Salama, N.R. (2008). *Helicobacter pylori* AddAB helicase-nuclease and RecA promote recombination-related DNA repair and survival during stomach colonization. Mol. Microbiol. *69*, 994–1007.

Andersen, L.P., and Rasmussen, L. (2009). *Helicobacter pylori*-coccoid forms and biofilm formation. FEMS Immunol. Med. Microbiol. *56*, 112–115.

Ausmees, N., Kuhn, J.R., and Jacobs-Wagner, C. (2003). The bacterial cytoskeleton: an intermediate filament-like function in cell shape. Cell *115*, 705–713.

Benaissa, M., Babin, P., Quellard, N., Pezennec, L., Cenatiempo, Y., and Fauchere, J.L. (1996). Changes in *Helicobacter pylori* ultrastructure and antigens during conversion from the bacillary to the coccoid form. Infect. Immun. *64*, 2331–2335.

Bendezu, F.O., Hale, C.A., Bernhardt, T.G., and de Boer, P.A. (2009). RodZ (YfgA) is required for proper assembly of the MreB actin cytoskeleton and cell shape in *E. coli*. EMBO J. *28*, 193–204.

Bennett-Lovsey, R.M., Herbert, A.D., Sternberg, M.J., and Kelley, L.A. (2008). Exploring the extremes of sequence/structure space with ensemble fold recognition in the program Phyre. Proteins *70*, 611–625.

Bove, J.M., Renaudin, J., Saillard, C., Foissac, X., and Garnier, M. (2003). *Spiroplasma citri*, a plant pathogenic molligute: relationships with its two hosts, the plant and the leafhopper vector. Annu. Rev. Phytopathol. *41*, 483–500.

Bromley, D.B., and Charon, N.W. (1979). Axial filament involvement in the motility of *Leptospira interrogans*. J. Bacteriol. *137*, 1406–1412.

Cabeen, M.T., Charbon, G., Vollmer, W., Born, P., Ausmees, N., Weibel, D.B., and Jacobs-Wagner, C. (2009). Bacterial cell curvature through mechanical control of cell growth. EMBO J. *28*, 1208–1219.

Cabeen, M.T., and Jacobs-Wagner, C. (2007). Skin and bones: the bacterial cytoskeleton, cell wall, and cell morphogenesis. J. Cell Biol. *179*, 381–387.

Celli, J.P., Turner, B.S., Afdhal, N.H., Keates, S., Ghiran, I., Kelly, C.P., Ewoldt, R.H., McKinley, G.H., So, P., Erramilli, S., et al. (2009). *Helicobacter pylori* moves through mucus by reducing mucin viscoelasticity. Proc. Natl. Acad. Sci. USA *106*, 14321–14326.

Costa, K., Bacher, G., Allmaier, G., Dominguez-Bello, M.G., Engstrand, L., Falk, P., de Pedro, M.A., and Garcia-del Portillo, F. (1999). The morphological transition of *Helicobacter pylori* cells from spiral to coccoid is preceded by a substantial modification of the cell wall. J. Bacteriol. *181*, 3710–3715.

Cover, T.L., and Blaser, M.J. (2009). *Helicobacter pylori* in health and disease. Gastroenterology *136*, 1863–1873.

Daniel, R.A., and Errington, J. (2003). Control of cell morphogenesis in bacteria: two distinct ways to make a rod-shaped cell. Cell *113*, 767–776.

de Pedro, M.A., Quintela, J.C., Holtje, J.V., and Schwarz, H. (1997). Murein segregation in *Escherichia coli*. J. Bacteriol. *179*, 2823–2834.

DeLoney, C.R., and Schiller, N.L. (1999). Competition of various beta-lactam antibiotics for the major penicillin-binding proteins of *Helicobacter pylori*: antibacterial activity and effects on bacterial morphology. Antimicrob. Agents Chemother. *43*, 2702–2709.

Denome, S.A., Elf, P.K., Henderson, T.A., Nelson, D.E., and Young, K.D. (1999). *Escherichia coli* mutants lacking all possible combinations of eight penicillin binding proteins: viability, characteristics, and implications for peptidoglycan synthesis. J. Bacteriol. *181*, 3981–3993.

Eaton, K.A., Suerbaum, S., Josenhans, C., and Krakowka, S. (1996). Colonization of gnotobiotic piglets by *Helicobacter pylori* deficient in two flagellin genes. Infect. Immun. *64*, 2445–2448.

Glauner, B., Holtje, J.V., and Schwarz, U. (1988). The composition of the murein of *Escherichia coli*. J. Biol. Chem. *263*, 10088–10095.

Goldstein, S.F., Charon, N.W., and Kreiling, J.A. (1994). *Borrelia burgdorferi* swims with a planar waveform similar to that of eukaryotic flagella. Proc. Natl. Acad. Sci. USA *91*, 3433–3437.

Goodwin, C.S., McCulloch, R.K., Armstrong, J.A., and Wee, S.H. (1985). Unusual cellular fatty acids and distinctive ultrastructure in a new spiral bacterium (*Campylobacter pyloridis*) from the human gastric mucosa. J. Med. Microbiol. *19*, 257–267.

Hay, N.A., Tipper, D.J., Gygi, D., and Hughes, C. (1999). A novel membrane protein influencing cell shape and multicellular swarming of *Proteus mirabilis*. J. Bacteriol. *181*, 2008–2016.

Hazell, S.L., Lee, A., Brady, L., and Hennessy, W. (1986). *Campylobacter pyloridis* and gastritis: association with intercellular spaces and adaptation to an environment of mucus as important factors in colonization of the gastric epithelium. J. Infect. Dis. *153*, 658–663.

Huang, K.C., Mukhopadhyay, R., Wen, B., Gitai, Z., and Wingreen, N.S. (2008). Cell shape and cell-wall organization in Gram-negative bacteria. Proc. Natl. Acad. Sci. USA *105*, 19282–19287.

Humbert, O., and Salama, N.R. (2008). The *Helicobacter pylori* HpyAXII restriction-modification system limits exogenous DNA uptake by targeting GTAC sites but shows asymmetric conservation of the DNA methyltransferase and restriction endonuclease components. Nucleic Acids Res. *36*, 6893–6906.

Jones, L.J., Carballido-Lopez, R., and Errington, J. (2001). Control of cell shape in bacteria: helical, actin-like filaments in *Bacillus subtilis*. Cell *104*, 913–922.

Kovach, M.E., Hughes, K.J., Everiss, K.D., and Peterson, K.M. (1994). Identification of a ToxR-activated gene, tagE, that lies within the accessory colonization factor gene cluster of *Vibrio cholerae* O395. Gene *148*, 91–95.

Kusters, J.G., van Vliet, A.H., and Kuipers, E.J. (2006). Pathogenesis of *Helicobacter pylori* infection. Clin. Microbiol. Rev. *19*, 449–490.

Lacayo, C.I., Pincus, Z., VanDuijn, M.M., Wilson, C.A., Fletcher, D.A., Gertler, F.B., Mogilner, A., and Theriot, J.A. (2007). Emergence of large-scale cell morphology and movement from local actin filament growth dynamics. PLoS Biol. *5*, e233.

Lowenthal, A.C., Hill, M., Sycuro, L.K., Mehmood, K., Salama, N.R., and Ottemann, K.M. (2009). Functional analysis of the Helicobacter pylori flagellar switch proteins. J. Bacteriol. *191*, 7147–7156.

Montecucco, C., and Rappuoli, R. (2001). Living dangerously: how Helicobacter pylori survives in the human stomach. Nat. Rev. Mol. Cell Biol. *2*, 457–466.

Odintsov, S.G., Sabala, I., Marcyjaniak, M., and Bochtler, M. (2004). Latent LytM at 1.3A resolution. J. Mol. Biol. *335*, 775–785.

Ragumani, S., Kumaran, D., Burley, S.K., and Swaminathan, S. (2008). Crystal structure of a putative lysostaphin peptidase from Vibrio cholerae. Proteins *72*, 1096–1103.

Rasband, W.S. (2009). ImageJ (http://rsb.info.nih.gov/ij).

Ruby, J.D., Li, H., Kuramitsu, H., Norris, S.J., Goldstein, S.F., Buttle, K.F., and Charon, N.W. (1997). Relationship of *Treponema denticola* periplasmic flagella to irregular cell morphology. J. Bacteriol. *179*, 1628–1635.

Salama, N.R., Shepherd, B., and Falkow, S. (2004). Global transposon mutagenesis and essential gene analysis of *Helicobacter pylori*. J. Bacteriol. *186*, 7926–7935.

Smeets, L.C., Bijlsma, J.J., Boomkens, S.Y., Vandenbroucke-Grauls, C.M., and Kusters, J.G. (2000). *comH*, a novel gene essential for natural transformation of *Helicobacter pylori*. J. Bacteriol. *182*, 3948–3954.

Tomb, J.F., White, O., Kerlavage, A.R., Clayton, R.A., Sutton, G.G., Fleischmann, R.D., Ketchum, K.A., Klenk, H.P., Gill, S., Dougherty, B.A., et al. (1997). The complete genome sequence of the gastric pathogen *Helicobacter pylori*. Nature *388*, 539–547.

Trachtenberg, S. (2004). Shaping and moving a spiroplasma. J. Mol. Microbiol. Biotechnol. *7*, 78–87.

Trachtenberg, S., Dorward, L.M., Speransky, V.V., Jaffe, H., Andrews, S.B., and Leapman, R.D. (2008). Structure of the cytoskeleton of *Spiroplasma melliferum* BC3 and its interactions with the cell membrane. J. Mol. Biol. *378*, 778–789.

Uehara, T., Dinh, T., and Bernhardt, T.G. (2009). LytM-domain factors are required for daughter cell separation and rapid ampicillin-induced lysis in *Escherichia coli*. J. Bacteriol. *191*, 5094–5107.

Varma, A., and Young, K.D. (2004). FtsZ collaborates with penicillin binding proteins to generate bacterial cell shape in *Escherichia coli*. J. Bacteriol. *186*, 6768–6774.

Vollmer, W., and Bertsche, U. (2008). Murein (peptidoglycan) structure, architecture and biosynthesis in *Escherichia coli*. Biochim. Biophys. Acta *1778*, 1714–1734.

Waidner, B., Specht, M., Dempwolff, F., Haeberer, K., Schaetzle, S., Speth, V., Kist, M., and Graumann, P.L. (2009). A novel system of cytoskeletal elements in the human pathogen *Helicobacter pylori*. PLoS Pathog. *5*, e1000669.

Williamson, D.L., Renaudin, J., and Bove, J.M. (1991). Nucleotide sequence of the *Spiroplasma citri* fibril protein gene. J. Bacteriol. *173*, 4353–4362.

Wolgemuth, C.W., Charon, N.W., Goldstein, S.F., and Goldstein, R.E. (2006). The flagellar cytoskeleton of the spirochetes. J. Mol. Microbiol. Biotechnol. *11*, 221–227.

Young, K.D. (2006). The selective value of bacterial shape. Microbiol. Mol. Biol. Rev. *70*, 660–703.